Brain Imaging and Behavior (2019) 13:1160–1171
https://doi.org/10.1007/s11682-018-9931-z

ORIGINAL RESEARCH

Radiation-induced hippocampal atrophy in patients with nasopharyngeal carcinoma early after radiotherapy: a longitudinal MR-based hippocampal subfield analysis

Xiaofei Lv[1] · Haoqiang He[1] · Yadi Yang[1] · Lujun Han[1] · Zheng Guo[2] · Hong Chen[1] · Jing Li[1] · Yingwei Qiu[3] · Chuanmiao Xie[1]

Published online: 27 July 2018

Abstract

Increasing evidence indicates that radiation-induced injury to the hippocampus may play a critical role in neurocognitive dysfunction in patients with nasopharyngeal carcinoma (NPC). However, few studies have assessed RT-induced hippocampal structural alterations in these patients early after radiotherapy (RT). In this study, 58 NPC patients were longitudinally followed up prior to treatment initiation as well as 3 and 6 months after RT, respectively. Twenty comparable normal controls were recruited and followed up in parallel. A novel magnetic resonance imaging (MRI)-based automated method was used to label hippocampal subfields. The linear mixed model was employed to evaluate longitudinal changes in the volumes of the whole hippocampus and seven hippocampal subfields. Time-dependent volume reduction was observed in the bilateral hippocampus, as well as in the bilateral granule cell layer (GCL), bilateral cornu ammonis 1 (CA1), bilateral molecular layer (ML), and bilateral subiculum (SUB) in NPC patients, but not in controls. Moreover, volume deficits in the bilateral hippocampus, bilateral GCL, and right ML showed dose-dependent patterns, and high volume losses in the bilateral hippocampus, bilateral GCL, left SUB, and right ML were associated with a rapid decline in cognitive function. Our findings demonstrated that the hippocampal subfields were selectively injured by irradiation-related early neurotoxic effects, which might account for cognitive impairment in NPC patients at an early stage after RT. Further, structural MRI could serve as a potential noninvasive imaging biomarker for the early detection of radiation effects on the hippocampus in NPC patients after RT.

Keywords Radiotherapy · Radiation-induced injury · Nasopharyngeal carcinoma · Hippocampus · Hippocampal subfields · Structural MRI

Xiaofei Lv, Haoqiang He and Yadi Yang contributed equally to this work.

Electronic supplementary material The online version of this article (https://doi.org/10.1007/s11682-018-9931-z) contains supplementary material, which is available to authorized users.

✉ Yingwei Qiu
qiuyw1201@gmail.com

✉ Chuanmiao Xie
xiechm@sysucc.org.cn

[1] Department of Medical Imaging, Sun Yat-sen University Cancer Center; State Key Laboratory of Oncology in South China; Collaborative Innovation Center for Cancer Medicine; Guangdong Key Laboratory of Nasopharyngeal Carcinoma Diagnosis and Therapy, Guangzhou, People's Republic of China

[2] Department of Oncology, The First Affiliated Hospital of Ganzhou Medical University, Ganzhou, Jiangxi, People's Republic of China

[3] Department of Radiology, The Third Affiliated Hospital of Guangzhou Medical University, Guangzhou Medical University, Guangzhou, People's Republic of China

Introduction

Nasopharyngeal carcinoma (NPC) is a prevalent malignant tumor in southern China, particularly in Guangdong Province (Torre et al. 2015). Radiotherapy (RT) is the standard radical treatment for non-disseminated NPC (Lee et al. 2015). The side effects of RT, such as RT-induced brain injury, have attracted increasing attention with the increase in survival rate and favorable outcomes of NPC. In the last few decades, late delayed injuries (typically beginning 6 months or more after RT) have been well documented as irreversible, and sometimes presented as necrosis of temporal lobes on routine medical imaging examinations (Mao et al. 2014). In contrast, RT-induced brain injury at an early stage after RT (acute and early delayed periods in the first 6 months after RT) is a significant sequela but largely unrecognized owing to its non-detectability by routine medical

imaging (Ding et al. 2018; Lin et al. 2017; Lv et al. 2014; Makale et al. 2017). Brain injury at the early stage not only potentially leads to cognitive dysfunction, but also exerts long-lasting effects and contributes to late delayed injury (Chapman et al. 2012; Makale et al. 2017).

Although the pathophysiology of brain injury at an early stage after RT is multifactorial and complex, the hippocampus is known to be particularly sensitive to the acute and subacute effects of radiation injury (Makale et al. 2017; Pospisil et al. 2017; Son et al. 2015). Increasing evidence indicates acute and subacute cognitive changes after RT, such as attention, memory, and executive function impairments, appear to be mediated through the injuries of neurogenic zones, including the hippocampus (Makale et al. 2017; Son et al. 2015). Anatomically, the hippocampus lies in the medial temporal lobe, which is often within the target volume that receives unnecessary radiation in patients with NPC (Mao et al. 2014). Theoretically, substantial advancements in treatment planning currently allow for precise control over delivered dose distributions. In the whole-brain RT setting, hippocampal-sparing RT techniques have shown promise for reducing early cognitive decline and improving the patients' quality life (Gondi et al. 2014). Unfortunately, no extra attention is paid to sparing the hippocampus, which is still not considered among organs at risk (OARs) when designing radiotherapeutic plans for patients with NPC (Sun et al. 2014). Identifying RT-induced hippocampal injury at an early stage after RT in patients with NPC may not only shed light on the complicated pathogenesis of RT-induced neurocognitive decline but also could offer the possibility of designing appropriate hippocampus dose-reduction strategies.

In recent years, investigators have used different magnetic resonance imaging (MRI)-based modalities to evaluate the effects of RT on the hippocampus (Chen et al. 2017; Decker et al. 2017; Farjam et al. 2015; Pospisil et al. 2017; Seibert et al. 2017). Of these, quantitative MRI has proved to be a promising and noninvasive imaging technique for analyzing RT-induced hippocampal structural damage (Decker et al. 2017; Seibert et al. 2017). A recent longitudinal study (Seibert et al. 2017) performed with a group of patients who underwent fractionated, partial brain RT for primary brain tumors showed significant hippocampal atrophy in the high-dose group 1 year after RT compared with the pre-RT baseline. The authors suggested that quantitative MRI could be investigated as a potential biomarker for the development of reliable dose constraints for improved cognitive outcomes (Seibert et al. 2017). Although RT-induced volume deficits of the hippocampus have been documented, these findings were derived primarily from studies evaluating patients with primary and metastatic brain tumors (Decker et al. 2017; Seibert et al. 2017). Different radiation fields and dosing schemes in patients with NPC and brain tumors might result in differences in hippocampal alterations between them. To date, little work has been conducted to assess RT-induced hippocampal volume alterations in patients with NPC.

Of note, the hippocampus is regarded as a highly complex and heterogeneous structure comprising a number of distinct, interacting sub-regions (Small et al. 2011). Histologically, these sub-regions are divided into the cornu ammonis (CA) subfields CA1–4, dentate gyrus (DG), fimbria, and adjacent subiculum (SUB) and presubiculum (Small et al. 2011). Previous studies have reported a non-uniform neuron loss rate of neuroplasticity across the hippocampal subfields, making the latter differentially susceptible to aging as well as neurological and psychiatric disorders (Cao et al. 2017; Iglesias et al. 2015; Small et al. 2011). Moreover, a recent study (Decker et al. 2017) observed that the majority of hippocampal subfields (DG-CA4, CA1, CA2–3, and stratum radiatum–lacunosum–moleculare) are smaller in pediatric brain tumor survivors after radio(chemo)therapy compared with typically developing children and adolescents, suggesting that specific subfields of the hippocampus might be vulnerable to cancer treatment. Thus, clear understanding of regional vulnerabilities in specific hippocampal subfields that occur at an early stage after RT in patients with NPC could provide in-depth insights into the pathophysiology of RT-induced structural injury, potentially enabling the optimization of treatment planning (such as RT target volume definition) to prevent and minimize additional secondary damage to the hippocampus.

Therefore, this study longitudinally assessed the volumes of the hippocampus and its subfields in a cohort of patients with NPC at an early stage after RT, using a novel MRI-based automated method to label the subfields. Based on previous studies (Decker et al. 2017; Seibert et al. 2017), it was hypothesized that patients with NPC who received RT would present volumetric reduction in the hippocampus and its subfields, and the hippocampal subfields would be differentially affected by RT at an early stage after RT.

Material and methods

Participants

The present prospective study was approved by the Institutional Review Board of the Sun Yat-sen University Cancer Center. Written informed consent was obtained from all individual participants included in the study. From December 2014 to November 2017, 58 patients (39 males and 19 females; aged 21–62 years, averaging 39.86 ± 9.58 years) with newly diagnosed, treatment-naïve NPC and 20 comparable normal controls (13 males and 7 females; aged 26–55 years, averaging 40.65 ± 9.76 years) were enrolled. The patients were diagnosed with nonkeratinizing undifferentiated NPC by histopathology. Each patient underwent a detailed

pretreatment evaluation, including physical examination; nasopharyngeal fiberoptic endoscopy; chest radiography; MRI scan of the nasopharynx, neck, and brain; abdominal sonography; whole-body bone scan; and positron emission tomography (PET)-computed tomography (CT) as indicated. All patients were staged according to the seventh edition of the International Union against Cancer/American Joint Committee on Cancer system. The overall function of each patient was assessed using the Karnofsky performance status (KPS) scale. The exclusion criteria for all participants were: age below 18 years or above 65 years, brain tumors, alcoholism, diabetes, neurological or psychiatric diseases, prior substantial head trauma, viral hepatitis, positive human immunodeficiency virus status, other major illnesses, left-handedness, and contraindications for MRI scanning. For NPC cases, additional exclusion criteria were: a KPS score lower than 80, intracranial invasion and distant metastases. The demographic and clinical characteristics of the NPC patients and normal controls assessed are summarized in Table 1.

Treatment

All patients were treated with intensity-modulated radiation therapy (IMRT) ($n = 53$) or tomography radiation therapy ($n = 5$) at the above institution as previously described (Mao et al. 2014; Sun et al. 2014; Yao et al. 2017). Target volumes were delineated slice by slice on treatment planning CT scans using an individualized delineation according to the institutional treatment protocol (Sun et al. 2014), in accordance with International Commission on Radiation Units and Measurements (ICRU) Reports 50 and 62. The prescribed regimen included a total dose of 68–70 Gy in 30–33 fractions at 2.12–2.33 Gy/fraction to the planning target volume (PTV) of the primary gross tumor volume (GTVnx), 60–70 Gy to the PTV of GTV of involved lymph nodes (GTVnd), 60–64 Gy to the PTV of the high-risk clinical target volume (CTV1), and 54–58 Gy to the PTV of the low-risk clinical target volume (CTV2). All patients received one fraction daily, 5 days per week. OARs, such as the temporal lobe, spinal cord, and parotid gland, were delineated according to a previous study (Sun et al. 2014). The dose received by each OAR was limited, as described in the Radiation Therapy Oncology Group 0225 protocol (Lee et al. 2009). The bilateral hippocampus was manually delineated on treatment planning CT axial images (Supplementary Fig. 1) by referring to T_1-weighted anatomical imaging, and the anatomic boundaries of the hippocampus were identified according to a previous protocol to calculate the dose–volume statistics for the bilateral hippocampus (Ghia et al. 2007). Dose evaluation was performed based on the data from the dose–volume histogram for the targets. The main evaluation parameters were maximum dose (D_{max}), mean dose (D_{mean}), and minimum dose (D_{min}) received by hippocampal tissues (Table 2 and Supplementary Fig. 1).

During the study, the institutional guidelines recommended only RT for stage I and concurrent chemoradiotherapy with or without neoadjuvant/adjuvant chemotherapy for stages II to IVB. The concurrent chemotherapy consisted of cisplatin/nedaplatin or paclitaxel administered weekly for at least 4–7 cycles or in weeks 1, 4, and 7 of radiation therapy. Neoadjuvant/adjuvant chemotherapy comprised cisplatin with 5-fluorouracil, cisplatin with docetaxel, cisplatin with paclitaxel, or cisplatin with 5-fluorouracil and docetaxel every 3 weeks for ≥2 cycles. Of the 58 patients, 3 (5.2%) underwent RT only, 22 (37.9%) were administered concurrent chemoradiotherapy, and 33 (56.9%) received a combination of neoadjuvant and concurrent chemoradiotherapy (Fig. 1).

MRI acquisition

All MRI data were collected on a GE Discovery MR750 3.0 Tesla scanner (GE Medical Systems, WI, USA) at the Department of Medical Imaging, Sun Yat-sen University Cancer Center. A tight but comfortable foam padding was used to minimize head motion. For each participant, routine MRI sequences, including thick-slice T2- and T1-weighted imaging as well as T2 fluid-attenuated inversion recovery imaging, were performed to ensure there were no visible brain lesions. Then, high-resolution structural MRI scan with T1 weighted three-dimensional brain volume imaging (3D-BRAVO) was conducted. Imaging parameters were: TR = 8.16 ms; TE = 3.18 ms; inversion time = 800 ms; flip angle =

Table 1 Demographic and clinical characteristics of patients with nasopharyngeal carcinoma (NPC) and normal controls at baseline

Demographic information	NPC patients	Normal controls	t/ χ^2 values	*P* values
Numbers	58	20	NA	NA
Age (year)*	39.86 ± 9.58	40.65 ± 9.76	0.316	0.753
Gender (male/female)	39/19	13/7	0.034	0.855
AJCC stage (I/II/III/IV)	1/7/27/23	NA	NA	NA
MoCA	28.98 ± 1.25 #	28.65 ± 0.93	0.993	0.325

*Data are mean ± standard deviation. # 50 patients underwent the MoCA test. AJCC, American Joint Committee on Cancer; RT, radiation therapy; MoCA, Montreal Cognitive Assessment; NA, not available

Table 2 Dose–volume statistics of the bilateral hippocampus for 58 patients with nasopharyngeal carcinoma treated with radiation therapy (Gy)

Hippocampus	Maximum dose (D_{max})	Minimum dose (D_{min})	Mean dose (D_{mean})
Left	47.90 ± 13.82	5.64 ± 3.96	20.35 ± 6.72
Right	49.51 ± 14.32	5.45 ± 3.44	20.63 ± 7.48

All data are presented as mean ± standard deviation

8°; acquisition matrix = 256 × 256; field of view = 256 × 256 mm^2; 176 sagittal slices; no inter-slice gap; and voxel size = 1 × 1 × 1 mm^3.

Neurocognitive tests

The Montreal Cognitive Assessment (MoCA, Beijing Version) tool was used to assess the general cognitive function of patients with NPC before and after treatment. Different cognitive domains were evaluated, including attention and concentration, executive functions, memory, language, visuoconstructional skills, conceptual thinking, and calculations and orientation. MoCA administration in each patient required approximately 10 min. The score range of MoCA was 0–30. The participants completed MoCA after an appropriate demonstration and explanation the day of MRI scanning.

Follow-up procedure

Patients with NPC were evaluated at the following time points to assess the dynamic alteration of hippocampal structure and cognitive function impairment at an early stage after RT: prior to treatment initiation (baseline, $n = 58$); 3 ($n = 45$) and 6 ($n = 32$) months following RT completion. In detail, 26 patients were assessed at baseline and the 3 month follow-up time point, 13 at baseline and the 6 month time point, and 19 at all three time points. Routine and high-resolution structural brain MRI scans were acquired at each time point. In addition, MoCA tests were performed with the patients' cooperation. Finally, 135 MRI and 105 MoCA data were collected. Details for NPC patient dropout are listed in Supplementary Materials. Meanwhile, all 20 normal controls completed MRI scans and MoCA measurements at the corresponding time points (baseline, three to four months, and six to seven months) during follow-up. Fig. 1 illustrates the follow-up of patients with NPC and normal controls.

Image processing

Preprocessing of the structural images obtained was performed using the open-source FreeSurfer pipeline (Dale et al. 1999; Fischl et al. 1999; Fischl et al. 2002; Fischl et al. 2004) (version 6.0, http://surfer.nmr.mgh.harvard.edu). Longitudinal data were further processed using a specialized longitudinal processing stream where unbiased subject-specific templates were created, and within-subject images for each time point were re-processed with common information from the template (Reuter et al. 2012). This was shown to reduce variability in within-subject morphological measures, hence resulting in higher statistical power and allowing the detection of small changes (Reuter et al. 2012).

A new automated algorithm from FreeSurfer was used to label the subfields (Fig. 2). This algorithm is based on a computational atlas built from ex vivo MRI data of post-mortem medial temporal tissue samples from 15 subjects, acquired at an average of 0.13-mm isotropic resolution on a 7-T MR scanner and an in vivo atlas providing information about adjacent extrahippocampal structures (Iglesias et al. 2015). Compared with the previous algorithm developed by FreeSurfer (Van Leemput et al. 2009), the volumes generated by this new algorithm were more comparable with histology-based measurements of the subfields (Iglesias et al. 2015). It also provided a more comprehensive, fine-grained segmentation of the structures of the hippocampus, and was able to reliably identify the granule cell layer (GCL) within the DG as well as the molecular layer (ML) within CA fields and the SUB.

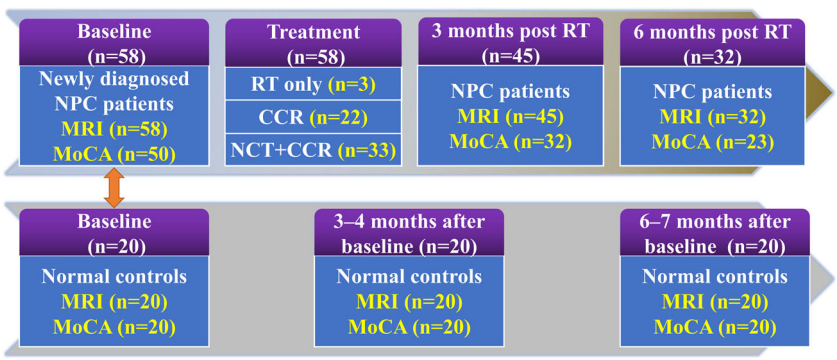

Fig. 1 Enrolment and follow-up procedures for patients with nasopharyngeal carcinoma (NPC) and normal controls. CCR, concurrent chemoradiotherapy; RT, radiation therapy; MoCA, performance of Montreal Cognitive Assessment; NCT, neoadjuvant /adjuvant chemotherapy, NPC, nasopharyngeal carcinoma

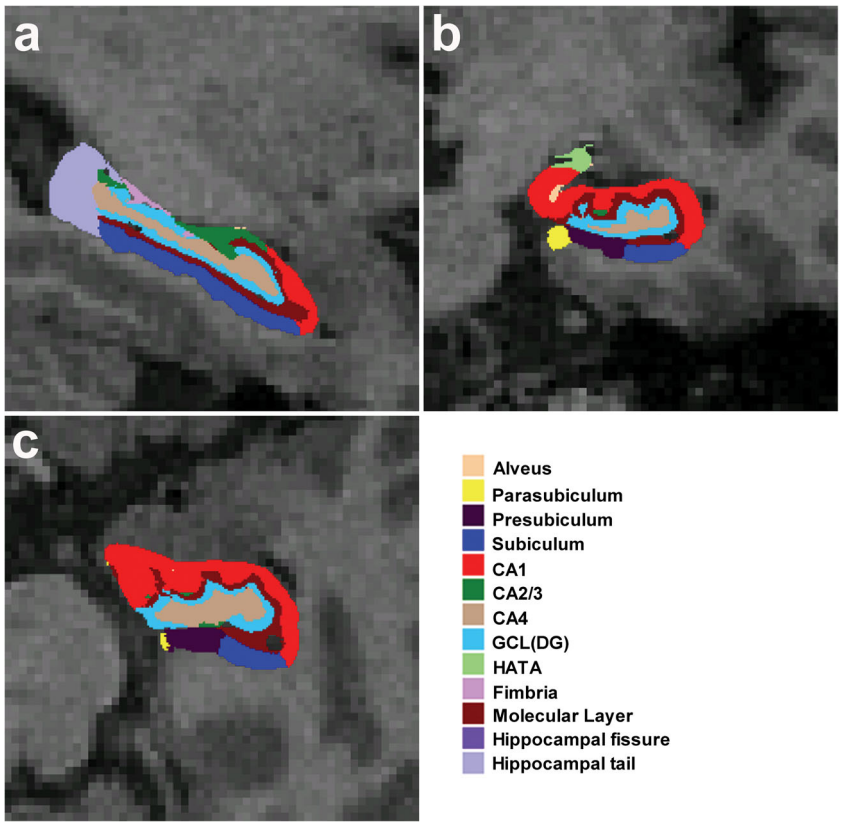

Fig. 2 Hippocampal subfield segmentation using a novel, MRI-based automated method. Subfield labels of the left hippocampus in a representative case with newly diagnosed nasopharyngeal carcinoma before treatment in the sagittal (**a**), coronal (**b**), and axial (**c**) planes are shown. CA, Cornu ammonis; DG, dentate gyrus; GCL, granule cell layer; HATA, hippocampus–amygdala transition area

The volumes of (i) the overall hippocampus generated using the widely used automated FreeSurfer subcortical segmentation script (based on the in vivo atlas) (Fischl et al. 2002) and (ii) seven structures considered subfields of the hippocampus (Iglesias et al. 2015) were measured. The seven fields included GCL, CA4, CA2/3 (CA2 and CA3 were combined in the atlas because of the lack of distinguishing MRI contrast), CA1, ML, hippocampal tail (the posterior end of the hippocampus, which included portions of the CA fields and DG undistinguishable with the MRI contrast), and the SUB.

Statistical analyses

All analyses were conducted with the open-source R software version 3.0.3 (R Team 2014). The authenticity of this article has been validated by uploading the key raw data onto the Research Data Deposit public platform (www.researchdata.org.cn), with the approval RDD number as RDDA2018000767.

Statistical analysis of NPC patients and normal controls at baseline

Pearson's chi-squared test was used to evaluate gender differences between the NPC patients and normal controls. Two-sample t-test was performed to assess differences in age and education level between the two groups. Univariate analysis was performed to assess differences in MoCA data as well as volumes of the hippocampus and hippocampal subfields between the two groups, with age and gender as covariates. In NPC patients, to evaluate the associations among different subfields, Pearson's correlation was performed among the volumes of different subfields at baseline in all patients.

Statistical analysis of changes in longitudinal hippocampus and its subfields during follow-up

The linear mixed model (Eq. (1)) was used to assess longitudinal changes in volumes of the hippocampus and its subfields (Bates et al. 2014), modeling fixed and random effects simultaneously and accounting for unequal sampling intervals and missing data (Long 2011).

$$\begin{aligned} Y_{ij} = {} & \gamma_{00} + \gamma_{01}\left(\text{gender}_j\right) + \gamma_{02}\left(\text{education}_j\right) + \gamma_{03}\left(\text{age}_j\right) \\ & + \gamma_{04}\left(\text{GM}_j\right) + \gamma_{10}\left(\text{time}_{ij}\right) + \gamma_{11}\left(\text{age}_j \times \text{time}_{ij}\right) \\ & + \mu_{0j} + \mu_{1j}\left(\text{time}_{ij}\right) + r_{ij} \end{aligned} \quad (1)$$

where Y_{ij} is the hippocampus or a given subfield for the ith patient with NPC on the jth follow-up visit after RT. The longitudinal variable represented the time interval (months) after RT completion. The pretreatment phase with quality hippocampal data for each participant was defined as baseline. Time always started from zero. Age represents the participant's age at baseline.

Gender (male or female) was a binary dummy variable, whereas age, education level, and total gray matter volume (GM) were grand-mean-centered versions of the respective variables. The linear mixed model highlighted the cross-level interaction effects (Morrell et al. 2009): the intercepts $(\gamma_{00} + \gamma_{01}\ (\text{gender}_{\ j}) + \gamma_{02}\ (\text{education}_{\ j}) + \gamma_{03}\ (\text{age}_{\ j}) + \gamma_{04}\ (\text{GM}_{\ j}) + \mu_{\ 0j})$ and the longitudinal changes $(\gamma_{10}\ (\text{time}_{\ ij}) + \gamma_{11}\ (\text{age}_{\ j} \times \text{time}_{\ ij}) + \mu_{1j}\ (\text{time}_{\ ij}))$ were unique to each participant (random effect μs), and this difference might be explained by individual differences (fixed effects γs). Specifically, time after completion of RT (time) might proceed at different rates depending on the cohort (age) [i.e., $\gamma_{\ 11}$ (age $_{j} \times$ time $_{ij}$)]. Longitudinal MoCA alterations were observed with the same model without the total GM variables. The same model was constructed for normal controls.

The longitudinal time effects on the hippocampus and its subfields, followed by MoCA scores, were examined using the proposed linear mixed model. Each of the volumetric measurements and MoCA scores was modeled separately.

The longitudinal effects related to time were reported to focus on time effects after RT completion (in patients with NPC) or after baseline (in normal controls) [i.e., $\gamma_{\ 10}$ and $\gamma_{\ 11}$ (Eq. (1)]. Statistically significant results at a threshold of $P < 0.05$ passing multiple comparison correction (hippocampus, corrected for 2 models; hippocampal subfields, corrected for 14 models) were reported. In cognitive models, time effects after completion of RT with $P < 0.05$ were reported.

Statistical analyses of associations of hippocampal volume alterations with hippocampal irradiation dose and cognitive alterations in patients with NPC

The present study focused on the hippocampus (and hippocampal subfields), which showed significant time effects after RT completion (i.e., time or its relevant interactions) and MoCA, to explore the associations of alterations of hippocampus and its subfields with cognition in longitudinal trends (Ng et al. 2016). First, the subject-specific slopes of the regression lines between time and the predicted volumes of the hippocampus (hippocampal subfields), total GM and MoCA were computed. This yielded $\beta_{\ 1i.\text{Volume}}$, $\beta_{1i.\text{GM}}$ and $\beta_{1i.\text{MoCA}}$, respectively. Next, these slopes were evaluated by multiple regression models associating hippocampus (hippocampal subfields) and MoCA after controlling for the changes of total GM:

$$\begin{aligned}\beta_{1i.\text{MoCA}} = {} & b_0 + b_1(\text{age}_i) + b_2(\text{gender}_i) + b_3(\text{education}_i) \\ & + b_4(\beta_{1i.\text{GMi}}) + b_5(\beta_{1i.\text{Volume}}) + b_6(\beta_{1i.\text{Volume}} \times \text{age}_i)\end{aligned} \quad (2)$$

where b_5 and b_6 are the estimated MoCA coefficient parameters of the hippocampus (hippocampal subfields). The current study also focused on the hippocampus (hippocampal subfields), which showed significant time effects after completion of RT (i.e., time or its relevant interactions), and irradiation doses of the ipsilateral hippocampus, to assess the associations of alterations of the hippocampus (hippocampal subfields) with the irradiation dose.

$$\begin{aligned}\beta_{1i.\text{Volume}} = {} & b_0 + b_1(\text{age}_i) + b_2(\text{gender}_i) \\ & + b_3(\text{education}_i) + b_4(\text{dose}_i)\end{aligned} \quad (3)$$

where b_4 is the estimated hippocampal (hippocampal subfields) volume-irradiation dose coefficient parameter.

Results

Demographic, clinical and hippocampal volume data at baseline

The demographic and clinical data of NPC patients and normal controls at baseline are shown in Table 1. There were no significant differences in age, gender, education level, and MoCA score (Table 1) as well as the volumes of the hippocampus and hippocampal subfields (Supplementary 1) between the two groups at baseline. The correlations among the volumes of different subfields at baseline in patients with NPC are listed in Supplementary Table 2.

Longitudinal changes in hippocampal and hippocampal subfield volumes

In NPC patients, significant longitudinal volume reductions in the bilateral hippocampus (left: $P = 6.359\text{e-}7$; right: $P = 8.335\text{e-}9$), bilateral CA1 (left: $P = 7.304\text{e-}5$; right: $P = 2.500\text{e-}6$), bilateral GCL (left: $P = 1.550\text{e-}4$; right: $P = 9.133\text{e-}4$), bilateral ML (left: $P = 2.060\text{e-}6$; right: $P = 1.491\text{e-}8$), and bilateral SUB (left: $P = 4.257\text{e-}7$; right: $P = 6.996\text{e-}6$) were observed during the first 6 months after RT, demonstrating a time-dependent atrophy pattern in these regions at an early stage after RT (Fig. 3, Supplementary Table 3). Similar results were obtained when the treatment regimen (with or without NCT) was considered an additional covariate (Supplementary Table 4). In normal controls, there were no significant longitudinal volume changes in the bilateral hippocampus and all hippocampal subfields (Supplementary Table 5).

Associations of changes in hippocampal and hippocampal subfield volumes with radiation dosage and neurocognitive performance

Significant negative correlations were observed between volume changes of the bilateral hippocampus (left: $P = 0.021$; right: $P < 0.001$), bilateral GCL (left: $P = 0.027$; right: $P < 0.001$), and right ML ($P < 0.001$) and the mean dose to the

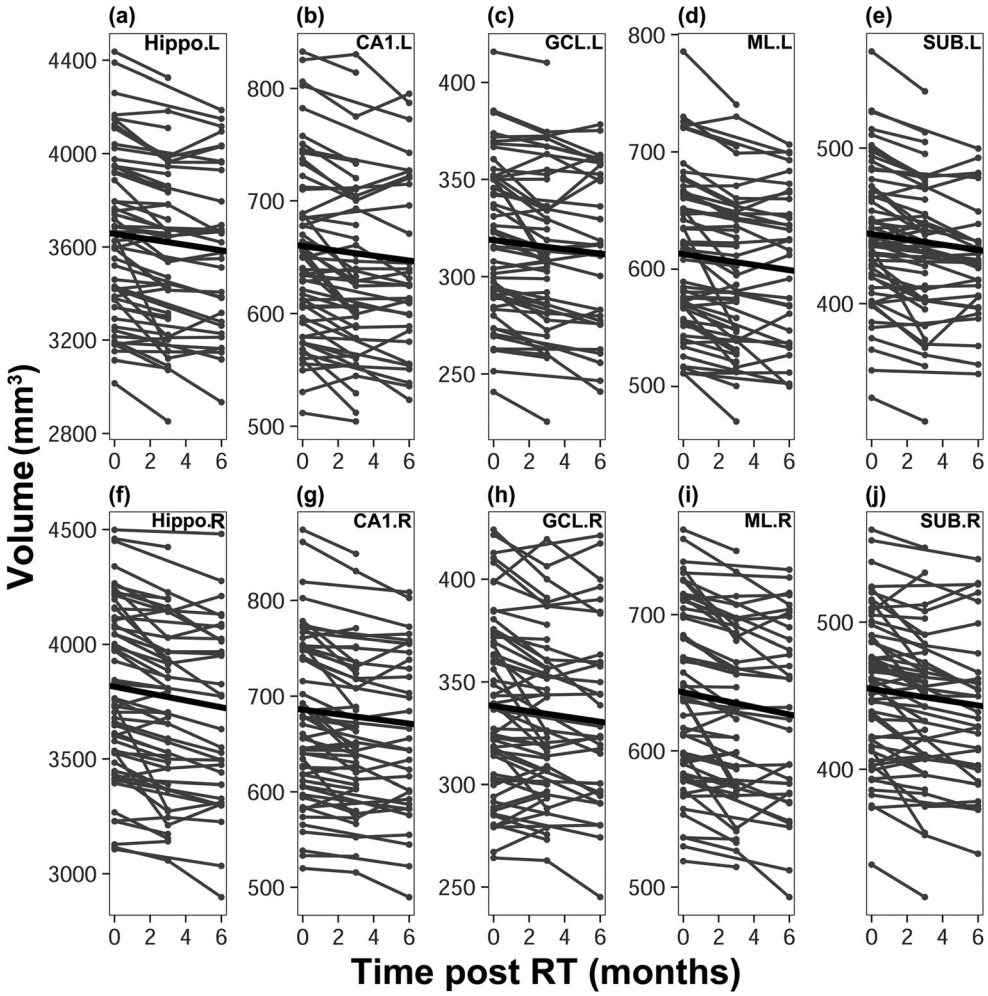

Fig. 3 Longitudinal changes in hippocampal and hippocampal subfield volumes in patients with nasopharyngeal carcinoma (NPC) before and at an early stage after RT. Spaghetti plots indicate the trajectories of volumes of the bilateral hippocampus and hippocampal subfields, displaying a time-dependent atrophy pattern in the bilateral hippo (**a** and **f**), bilateral CA1 (**b** and **g**), bilateral GCL (**c** and **h**), bilateral ML (**d** and **i**), and bilateral SUB (**e** and **j**) in patients with NPC from baseline to 3 and 6 months after RT, respectively. Bold lines represent the groups' mean linear regression lines. CA, Cornu ammonis; GCL, granule cell layer; hippo, hippocampus; ML, molecular layer; RT, radiation therapy; SUB, subiculum

ipsilateral hippocampus (Fig. 4). In addition, elevated volume losses in the bilateral hippocampus (left: $P = 0.017$; right: $P = 0.002$), bilateral GCL (left: $P = 0.011$; right: $P = 0.022$), left SUB ($P = 0.018$), and right ML ($P = 0.002$) were associated with a rapid decline in cognitive function evaluated by MoCA in patients with NPC (Fig. 5).

Discussion

This longitudinal study explored early RT-related neurotoxicity in hippocampal subfields using structural MRI in a relatively large cohort of patients with NPC in the first 6 months after RT. Using a novel, MR-based automated hippocampal segmentation approach, the current study found significant, time-dependent atrophy in the bilateral hippocampus, as well as the bilateral GCL, CA1, ML, and SUB in NPC patients but not in normal controls, suggesting that atrophy of the hippocampus and its subfields in NPC patients is most likely due to treatment (RT), rather than being an age-related effect. Importantly, volume changes in the bilateral hippocampus, bilateral GCL, and right ML were correlated with the radiation dose of the ipsilateral hippocampus, indicating a dose-dependent atrophy of these regions. Intriguingly, this study also found that higher volume losses in the bilateral hippocampus, bilateral GCL, left SUB, and right ML were associated with a faster decline in cognitive function as evaluated by MoCA, indicating that atrophy of the hippocampal and selective subfields might underlie cognitive impairment in patients with NPC. These findings might have important implications in the pathophysiological understanding of hippocampal structural injury in patients with NPC administered RT.

Increasing evidence reveals global hippocampal atrophy induced by long-term effects of radiation (Decker et al. 2017; Seibert et al. 2017). However, few studies have focused on the early effects of RT on hippocampal morphology. MRI-based hippocampal volumetric analysis in patients with NPC revealed time-dependent bilateral hippocampal atrophy in the first 6 months after RT completion in the present study. The findings of hippocampal abnormalities at an early stage after RT were in line with increasing evidence from recent studies using other MRI modalities, such as dynamic contrast-enhanced (DCE) MRI (Farjam et al. 2015), proton magnetic resonance spectroscopy (MRS) imaging (Pospisil et al. 2017),

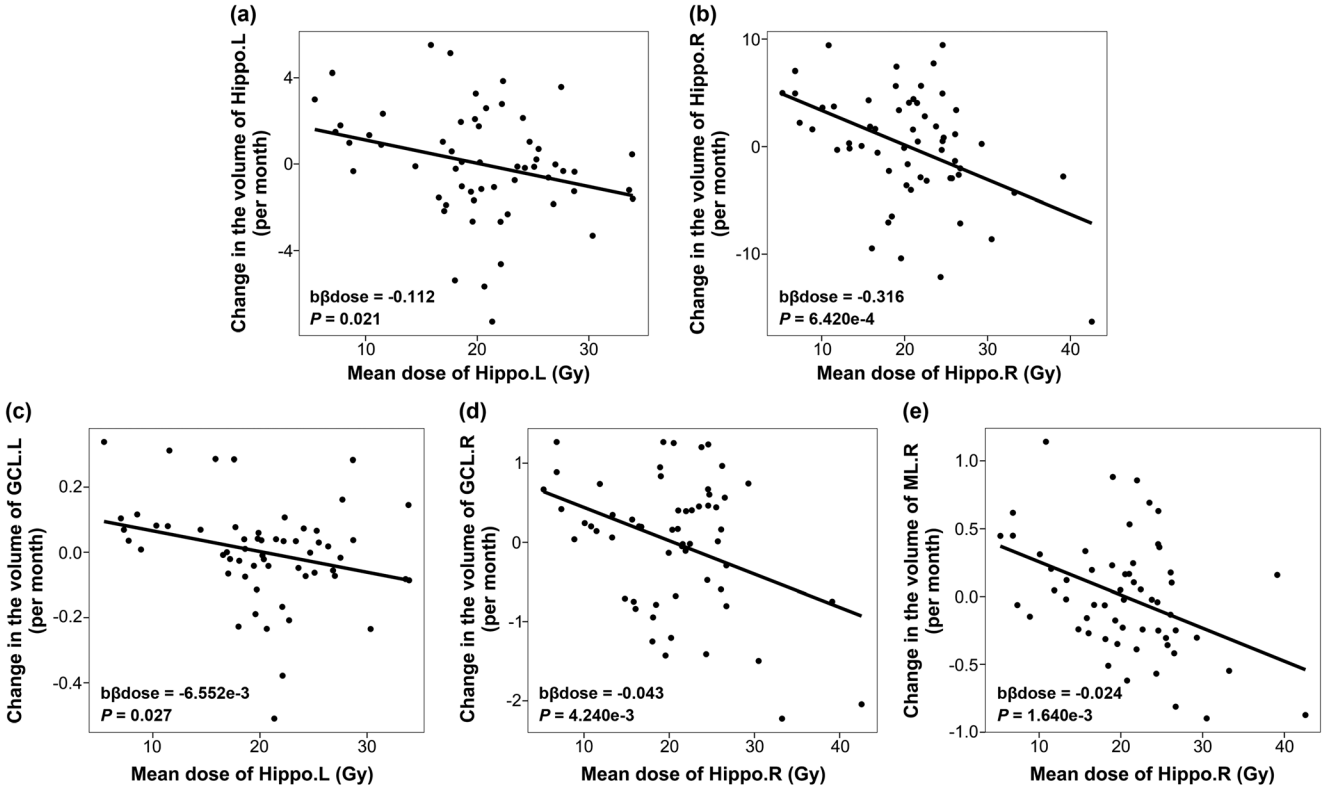

Fig. 4 Associations of changes in hippocampal and hippocampal subfield volumes with radiation dosage. Dose-dependent volume reductions of the bilateral hippo (**a** and **b**), bilateral GCL (**c** and **d**), and right ML. Each point represents the subject-level longitudinal change in hippocampal or hippocampal subfield volume (*y*-axis; higher values indicate greater volume loss) and the corresponding mean dose to the ipsilateral hippocampus (*x*-axis). GCL, granule cell layer; hippo, hippocampus; L, left; ML, molecular layer; R, right

and resting-state functional MRI (Chen et al. 2017), which have shown increased blood–brain barrier permeability and neuronal loss in the hippocampus, as well as abnormal functional connectivity of hippocampal-related cortices at time points earlier than 6 months. Moreover, loss of total hippocampal volume at an early stage after RT was also consistent with a previous longitudinal study in humans (Simo et al. 2016). Specifically, patients with small cell lung cancer showed a decreased GM volume in the hippocampus 3 months after prophylactic cranial radiation treatment compared with baseline.

Elucidating the cellular determinants of deceased subfield volumes in patients with NPC after RT is challenging because few studies have related histological features to hippocampal subfield volumes. The present study found that the time-dependent volume decreased significantly in GCL within the DG. This finding was consistent with previous studies reporting smaller DG volumes in irradiated rodents (Gazdzinski et al. 2012; Hellstrom et al. 2009) and humans (Decker et al. 2017). The DG is a key structure in the hippocampus that serves as the site of neurogenesis, and consists of the GCL and subgranular layer. It is known to be extremely sensitive to radiation exposure (Balentova and Adamkov 2015; Son et al. 2015). Previous studies showed that radiation to the hippocampus would result in increased apoptosis in the subgranular zone of the DG, reduced proliferation of the surviving neural stem cells, reduced differentiation into neurons (Greene-Schloesser et al. 2012), and time-dependent alterations in dendritic complexity, spine density, and morphology in the DG (Parihar and Limoli 2013) at an early stage after RT. Fewer DG neurons have been suggested to correlate with smaller volumes (Bobinski et al. 2000). Thus, GCL atrophy in the DG at an early stage after RT in patients with NPC might reflect increased apoptosis and reduced neurogenesis.

It is not surprising that CA1 showed a reduction in time-dependent volumes at an early stage after RT, as a considerable number of studies have examined pathology in CA1, highlighting its vulnerability to conditions involving vascular pathology and hypoxic ischemia (Hatanpaa et al. 2014; Small et al. 2011). Recently, significantly smaller CA1 volume was also observed in pediatric brain tumor survivors after radio(-chemo)therapy, suggesting that CA1 might be vulnerable to brain cancer treatment (Decker et al. 2017). Previous studies (Balentova and Adamkov 2015; Brown et al. 2005; Makale et al. 2017) indicated that RT-induced early injury is closely linked to vascular damage, represented by vessel dilatation, loss of endothelial cells, enlargement of endothelial cell nuclei, vessel wall thickening, decrease in vessel density and length, increase in vessel permeability, and altered integrity of endothelial tight junctions. Moreover, profound vascular rarefaction and hypoxia were observed in the hippocampus

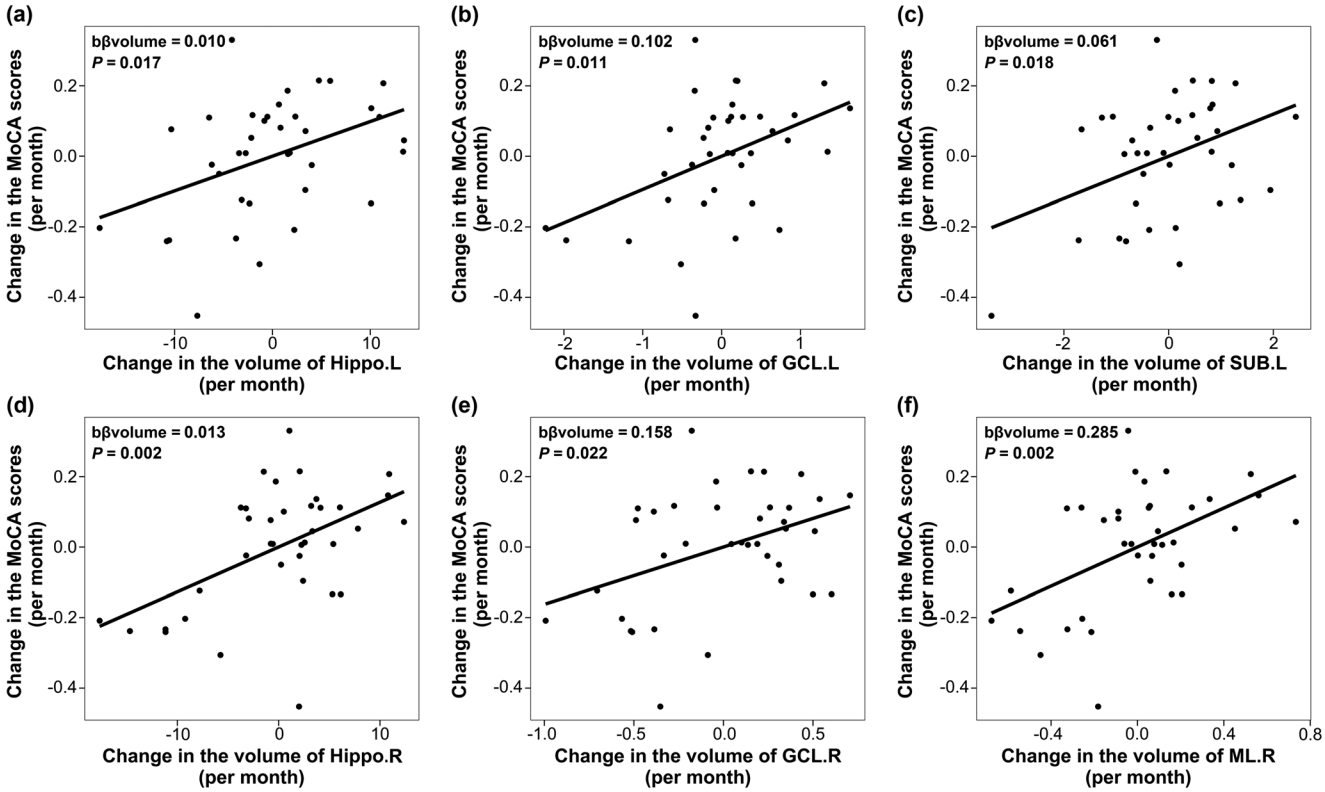

Fig. 5 Associations of changes in hippocampal and hippocampal subfield volumes with MoCA performance. Greater volume losses in the bilateral hippo (**a** and **b**), bilateral GCL (**c** and **d**), left SUB (**e**), and right ML (**f**) were associated with a faster decline in cognitive function as evaluated by MoCA. Each point indicates the subject-level longitudinal change in the MoCA (*y*-axis; lower values indicate a faster decline in MoCA) and the corresponding longitudinal change in hippocampal and hippocampal subfield volumes (*x*-axis; higher values indicate greater volume loss). GCL, granule cell layer; hippo, hippocampus; L, left; ML, molecular layer; MoCA, performance of Montreal Cognitive Assessment; R, right; SUB, subiculum

at an early stage after irradiation (Warrington et al. 2011). Using DCE-MRI, a dose-dependent increase in K^{trans} mean values, which reflect blood–brain barrier permeability, was observed in the hippocampus as early as 1 month after RT completion in patients with brain tumors, providing evidence that radiation-induced vascular injury in the hippocampus occurs at an early stage after RT (Farjam et al. 2015). Based on these findings, it was speculated that the regional vulnerabilities of volume deficit in the CA1 subfield at an early stage after RT in patients with NPC might be associated with early radiation effects on vascular injury.

The time-dependent atrophy in the ML at an early stage after RT in patients with NPC was a novel finding, given that the ML was not labeled using the previous automated method based on an in vivo atlas. The ML labeled by this new method included the ML of the SUB and CA fields (Iglesias et al. 2015). Specifically, the ML in this algorithm referred to a band comprising the stratum radiatum, lacunosum moleculare, hippocampal sulcus, and the ML of the DG (Cao et al. 2017), consisting of interneurons or synaptic connections of these subfields (Chittajallu et al. 2007). These interneurons are essential in regulating the activities within the hippocampus (Chittajallu et al. 2007). Although limited studies have explored the vulnerability of the hippocampal ML to early radiation in humans, recent animal studies have linked early radiation exposure to the loss of drebrin from dendritic spines (Puspitasari et al. 2016), as well as changes in synaptic proteins in the ML (Parihar and Limoli 2013), which promote degeneration and compromise neuronal connectivity (Parihar and Limoli 2013). Thus, it was presumed that these RT-induced alterations might be related to the reduced ML volumes observed in patients with NPC at an early stage after RT. However, further studies are needed to elucidate the underlying biological mechanisms.

The present study also revealed a time-dependent volume reduction in the SUB field, which is thought to serve as a major gateway to relay hippocampal output to a number of brain regions, including entorhinal and parahippocampal cortices, as well as limbic and associative cortices (O'Mara 2005). Although limited studies have assessed the irradiation effect on the SUB, a previous animal study (Chmielewski et al. 2016) showed reduced dendritic complexity and markedly elevated PSD-95 in the SUB in mouse brain 1 month after exposure to low-dose proton irradiation. Thus, it was suspected that the SUB atrophy observed in the present study might be, at least partly, associated with radiation-induced

disruption of neuronal structure and synaptic integrity in patients with NPC at an early stage after RT.

Furthermore, this study observed a radiation dose-dependent atrophy in the bilateral hippocampus, bilateral GCL, and right ML. Irradiation dose-dependent brain volume deficit has also been well documented in previous studies (Karunamuni et al. 2016; Lv et al. 2014; Seibert et al. 2017). Moreover, dose-dependent hippocampal injury has also been validated by previous studies in animal models (Parihar and Limoli 2013) and patients with brain tumors (Farjam et al. 2015; Seibert et al. 2017). For instance, Seibert et al. (Seibert et al. 2017) showed radiation dose-dependent atrophy in the hippocampus after treatment of patients who underwent fractionated, partial brain RT for primary brain tumors. Thus, the present longitudinal study suggested that atrophy of the hippocampus and its subfields is primarily induced by radiation in patients with NPC, indicating that a safe dose is important to protect these vulnerable regions.

Importantly, this study demonstrated that cognitive function was significantly impaired over a period in patients with NPC at an early stage after RT, in agreement with RT-related cognitive impairment revealed by previous studies (Makale et al. 2017; Pospisil et al. 2017). Moreover, this study found that reduced volumes in the bilateral hippocampus and its several subfields (bilateral GCL, left SUB, and right ML) were significantly associated with worse MoCA performance, providing more evidence that volume deficit in the hippocampus and its subfields was associated with cognitive impairment in patients with NPC at an early stage after RT. The above findings corroborated a previous MRS study (Pospisil et al. 2017), which showed correlations between declined cognitive function and changes in hippocampal metabolite concentrations 4 months after RT. However, further studies on this issue are required considering the rarity of reports evaluating cognitive deficit and RT-induced structural changes in hippocampal subfields in humans.

Despite its prospective nature, the present study had several limitations. First, MoCA is a brief cognitive screening tool (Nasreddine et al. 2005), and a complex cognitive evaluation method with the ability to detect changes in subfield-related cognitive domains is essential for future studies. Given that impairments of various subfields (GCL, CA1, ML and SUB) were related to irradiation in the current study, the corresponding cognitive functions, such as learning and early retrieval memory for GCL (Mueller et al. 2011), late retrieval and consolidation memory for CA1 (Mueller et al. 2011), spatial learning and memory for ML (Santos-Filho et al. 2014), and processing of spatial, mnemonic and movement information for SUB (O'Mara 2005), should be assessed and customized in the future. Secondly, it is worth mentioning that most patients with NPC received concurrent chemotherapy with or without a neoadjuvant chemotherapeutic regimen. Reportedly, chemotherapy itself might also cause neural progenitor cells to lose self-renewal capacity in the hippocampus (Dietrich et al. 2015). However, in the present study, similar longitudinal volume changes were found when the treatment regimen (with or without neoadjuvant chemotherapy) was considered a covariate. Moreover, a dose-dependent response was found in the hippocampus and its several subfields. Thus, these abnormalities might mainly be due to RT, while chemotherapy-related effects, if any, might be relatively small. Future studies should assess an RT only group to elucidate such effects.

Conclusions

In summary, this study reported time-dependent volume reductions in the bilateral hippocampus and its subfields (bilateral GCL, CA1, ML, and SUB) in patients with NPC at an early stage after RT. Moreover, volume deficits in the bilateral hippocampus, bilateral GCL, and right ML were dose dependent, and greater volume losses in the bilateral hippocampus and its several subfields were associated with a faster decline in cognitive function. These findings provided evidence that RT is associated with early neurotoxic effects on the hippocampal structure and subfields, which might underlie the cognitive impairment observed in patients with NPC at an early stage after RT. Hence, a hippocampal-sparing strategy should be considered when designing RT plans for patients with NPC to avoid the most vulnerable subfield and achieve an across-the-board preservation of related cognitive function. Meanwhile, the current findings also suggested that structural MRI could serve as a potential noninvasive imaging biomarker for the early detection of radiation effects on the hippocampus in patients with NPC at an early stage after RT.

Funding This work was funded by grants from the Natural Scientific Foundation of China (grant numbers: 81401399, 81560283, and 81201084), Natural Scientific Foundation of Jiangxi Province, China (grant number: 20151BAB205049), Fundamental Research Funds for the Central Universities (Grant number: 15ykpy35), and Medical Scientific Research Foundation of Guangdong Province (Grant number: B2014162).

Compliance with ethical standards

Conflict of interest The authors declare that they have no conflict of interest.

Ethical approval All procedures performed in studies involving human participants were in accordance with the ethical standards of the institutional and/or national research committee and with the 1964 Helsinki declaration and its later amendments or comparable ethical standards.

Informed consent Informed consent was obtained from all individual participants included in the study.

References

Balentova, S., & Adamkov, M. (2015). Molecular, cellular and functional effects of radiation-induced brain injury: A review. *International Journal of Molecular Sciences, 16*(11), 27796–27815. https://doi.org/10.3390/ijms161126068.

Bates, D., Mächler M., Bolker B., & Walker S. (2014). Fitting linear mixed-effects models using lme4. arXiv:1406.5823 [stat.CO].

Bobinski, M., de Leon M. J., Wegiel J., Desanti S., Convit A., Saint L. L., et al. (2000). The histological validation of post mortem magnetic resonance imaging-determined hippocampal volume in Alzheimer's disease. Neuroscience, 95(3), 721–725.

Brown, W. R., Thore, C. R., Moody, D. M., Robbins, M. E., & Wheeler, K. T. (2005). Vascular damage after fractionated whole-brain irradiation in rats. *Radiation Research, 164*(5), 662–668.

Cao, B., Passos I. C., Mwangi B., Amaral-Silva H., Tannous J., Wu M. J., et al. (2017). Hippocampal subfield volumes in mood disorders. Molecular Psychiatry, 22(9), 1352–1358. https://doi.org/10.1038/mp.2016.262.

Chapman, C. H., Nagesh V., Sundgren P. C., Buchtel H., Chenevert T. L., Junck L., et al. (2012). Diffusion tensor imaging of normal-appearing white matter as biomarker for radiation-induced late delayed cognitive decline. International Journal of Radiation Oncology, Biology, Physics, 82(5), 2033–2040. https://doi.org/10.1016/j.ijrobp.2011.01.068.

Chen, S. C., Abe Y., Fang P. T., Hsieh Y. J., Yang Y. I., Lu T. Y., et al. (2017). Prognosis of hippocampal function after sub-lethal irradiation brain injury in patients with nasopharyngeal carcinoma. Scientific Reports, 7(1), 14697. https://doi.org/10.1038/s41598-017-13972-2.

Chittajallu, R., Kunze, A., Mangin, J. M., & Gallo, V. (2007). Differential synaptic integration of interneurons in the outer and inner molecular layers of the developing dentate gyrus. *The Journal of Neuroscience, 27*(31), 8219–8225. https://doi.org/10.1523/JNEUROSCI.2476-07.2007.

Chmielewski, N. N., Caressi, C., Giedzinski, E., Parihar, V. K., & Limoli, C. L. (2016). Contrasting the effects of proton irradiation on dendritic complexity of subiculum neurons in wild type and MCAT mice. *Environmental and Molecular Mutagenesis, 57*(5), 364–371. https://doi.org/10.1002/em.22006.

Dale, A. M., Fischl, B., & Sereno, M. I. (1999). Cortical surface-based analysis. I. Segmentation and surface reconstruction. *NeuroImage, 9*(2), 179–194. https://doi.org/10.1006/nimg.1998.0395.

Decker, A. L., Szulc K. U., Bouffet E., Laughlin S., Chakravarty M. M., Skocic J., et al. (2017). Smaller hippocampal subfield volumes predict verbal associative memory in pediatric brain tumor survivors. Hippocampus, 27(11), 1140–1154. https://doi.org/10.1002/hipo.22758.

Dietrich, J., Prust, M., & Kaiser, J. (2015). Chemotherapy, cognitive impairment and hippocampal toxicity. *Neuroscience, 309*(26), 224–232. https://doi.org/10.1016/j.neuroscience.2015.06.016.

Ding, Z., Zhang H., Lv X. F., Xie F., Liu L., Qiu S., et al. (2018). Radiation-induced brain structural and functional abnormalities in presymptomatic phase and outcome prediction. Human Brain Mapping, 39(1), 407–427. https://doi.org/10.1002/hbm.23852.

Farjam, R., Pramanik P., Aryal M. P., Srinivasan A., Chapman C. H., Tsien C. I., et al. (2015). A radiation-induced hippocampal vascular injury surrogate marker predicts late neurocognitive dysfunction. International Journal of Radiation Oncology, Biology, Physics, 93(4), 908–915. https://doi.org/10.1016/j.ijrobp.2015.08.014.

Fischl, B., Sereno, M. I., & Dale, A. M. (1999). Cortical surface-based analysis. II: Inflation, flattening, and a surface-based coordinate system. *NeuroImage, 9*(2), 195–207. https://doi.org/10.1006/nimg.1998.0396.

Fischl, B., Salat D. H., Busa E., Albert M., Dieterich M., Haselgrove C., et al. (2002). Whole brain segmentation: Automated labeling of neuroanatomical structures in the human brain. Neuron, 33(3), 341–355.

Fischl, B., van der Kouwe A., Destrieux C., Halgren E., Segonne F., Salat D. H., et al. (2004). Automatically parcellating the human cerebral cortex. Cerebral Cortex, 14(1), 11–22.

Gazdzinski, L. M., Cormier, K., Lu, F. G., Lerch, J. P., Wong, C. S., & Nieman, B. J. (2012). Radiation-induced alterations in mouse brain development characterized by magnetic resonance imaging. *International Journal of Radiation Oncology, Biology, Physics, 84*(5), e631–e638. https://doi.org/10.1016/j.ijrobp.2012.06.053.

Ghia, A., Tome W. A., Thomas S., Cannon G., Khuntia D., Kuo J. S., et al. (2007). Distribution of brain metastases in relation to the hippocampus: Implications for neurocognitive functional preservation. International Journal of Radiation Oncology, Biology, Physics, 68(4), 971–977. https://doi.org/10.1016/j.ijrobp.2007.02.016.

Gondi, V., Pugh S. L., Tome W. A., Caine C., Corn B., Kanner A., et al. (2014). Preservation of memory with conformal avoidance of the hippocampal neural stem-cell compartment during whole-brain radiotherapy for brain metastases (RTOG 0933): A phase II multi-institutional trial. Journal of Clinical Oncology, 32(34), 3810–3816. https://doi.org/10.1200/JCO.2014.57.2909.

Greene-Schloesser, D., Robbins, M. E., Peiffer, A. M., Shaw, E. G., Wheeler, K. T., & Chan, M. D. (2012). Radiation-induced brain injury: A review. *Frontiers in Oncology, 2*, 73. https://doi.org/10.3389/fonc.2012.00073.

Hatanpaa, K. J., Raisanen J. M., Herndon E., Burns D. K., Foong C., Habib A. A., et al. (2014). Hippocampal sclerosis in dementia, epilepsy, and ischemic injury: Differential vulnerability of hippocampal subfields. Journal of Neuropathology and Experimental Neurology, 73(2), 136–142. https://doi.org/10.1097/OPX.0000000000000170.

Hellstrom, N. A., Bjork-Eriksson, T., Blomgren, K., & Kuhn, H. G. (2009). Differential recovery of neural stem cells in the subventricular zone and dentate gyrus after ionizing radiation. *Stem Cells, 27*(3), 634–641. https://doi.org/10.1634/stemcells.2008-0732.

Iglesias, J. E., Augustinack J. C., Nguyen K., Player C. M., Player A., Wright M., et al. (2015). A computational atlas of the hippocampal formation using ex vivo, ultra-high resolution MRI: Application to adaptive segmentation of in vivo MRI. NeuroImage, 115, 117–137. https://doi.org/10.1016/j.neuroimage.2015.04.042.

Karunamuni, R., Bartsch H., White N. S., Moiseenko V., Carmona R., Marshall D. C., et al. (2016). Dose-dependent cortical thinning after partial brain irradiation in high-grade glioma. International Journal of Radiation Oncology, Biology, Physics, 94(2), 297–304. https://doi.org/10.1016/j.ijrobp.2015.10.026.

Lee, N., Harris J., Garden A. S., Straube W., Glisson B., Xia P., et al. (2009). Intensity-modulated radiation therapy with or without chemotherapy for nasopharyngeal carcinoma: Radiation therapy oncology group phase II trial 0225. Journal of Clinical Oncology, 27(22), 3684–3690. https://doi.org/10.1200/JCO.2008.19.9109.

Lee, A. W., Ma, B. B., Ng, W. T., & Chan, A. T. (2015). Management of Nasopharyngeal Carcinoma: Current practice and future perspective. *Journal of Clinical Oncology, 33*(29), 3356–3364. https://doi.org/10.1200/JCO.2015.60.9347.

Lin, J., Lv X., Niu M., Liu L., Chen J., Xie F., et al. (2017). Radiation-induced abnormal cortical thickness in patients with nasopharyngeal carcinoma after radiotherapy. NeuroImage: Clinical, 14, 610–621. https://doi.org/10.1016/j.nicl.2017.02.025.

Long, J. D. (2011). *Longitudinal data analysis for the behavioral sciences using R*. Thousand Oaks, CA: Sage.

Lv, X. F., Zheng X. L., Zhang W. D., Liu L. Z., Zhang Y. M., Chen M. Y., et al. (2014). Radiation-induced changes in normal-appearing gray matter in patients with nasopharyngeal carcinoma: A magnetic

resonance imaging voxel-based morphometry study. Neuroradiology, 56(5), 423–430. https://doi.org/10.1007/s00234-014-1338-y.

Makale, M. T., McDonald, C. R., Hattangadi-Gluth, J. A., & Kesari, S. (2017). Mechanisms of radiotherapy-associated cognitive disability in patients with brain tumours. *Nature Reviews Neurology, 13*(1), 52–64. https://doi.org/10.1038/nrneurol.2016.185.

Mao, Y. P., Zhou G. Q., Liu L. Z., Guo R., Sun Y., Li L., et al. (2014). Comparison of radiological and clinical features of temporal lobe necrosis in nasopharyngeal carcinoma patients treated with 2D radiotherapy or intensity-modulated radiotherapy. British Journal of Cancer, 110(11), 2633–2639. https://doi.org/10.1038/bjc.2014.243.

Morrell, C. H., Brant, L. J., & Ferrucci, L. (2009). Model choice can obscure results in longitudinal studies. *The Journals of Gerontology Series A: Biological Sciences and Medical Sciences, 64*(2), 215–222. https://doi.org/10.1093/gerona/gln024.

Mueller, S. G., Chao, L. L., Berman, B., & Weiner, M. W. (2011). Evidence for functional specialization of hippocampal subfields detected by MR subfield volumetry on high resolution images at 4 T. *NeuroImage, 56*(3), 851–857. https://doi.org/10.1016/j.neuroimage.2011.03.028.

Nasreddine, Z. S., Phillips N. A., Bedirian V., Charbonneau S., Whitehead V., Collin I., et al. (2005). The Montreal cognitive assessment, MoCA: A brief screening tool for mild cognitive impairment. Journal of the American Geriatrics Society, 53(4), 695–699. https://doi.org/10.1111/j.1532-5415.2005.53221.x.

Ng, K. K., Lo, J. C., Lim, J. K., Chee, M. W., & Zhou, J. (2016). Reduced functional segregation between the default mode network and the executive control network in healthy older adults: A longitudinal study. *NeuroImage, 133*, 321–330. https://doi.org/10.1016/j.neuroimage.2016.03.029.

O'Mara, S. (2005). The subiculum: What it does, what it might do, and what neuroanatomy has yet to tell us. *Journal of Anatomy, 207*(3), 271–282. https://doi.org/10.1111/j.1469-7580.2005.00446.x.

Parihar, V. K., & Limoli, C. L. (2013). Cranial irradiation compromises neuronal architecture in the hippocampus. *Proceedings of the National Academy of Sciences of the United States of America, 110*(31), 12822–12827. https://doi.org/10.1073/pnas.1307301110.

Pospisil, P., Kazda T., Hynkova L., Bulik M., Dobiaskova M., Burkon P., et al. (2017). Post-WBRT cognitive impairment and hippocampal neuronal depletion measured by in vivo metabolic MR spectroscopy: Results of prospective investigational study. Radiotherapy and Oncology, 122(3), 373–379. https://doi.org/10.1016/j.radonc.2016.12.013.

Puspitasari, A., Koganezawa N., Ishizuka Y., Kojima N., Tanaka N., Nakano T., et al. (2016). X irradiation induces acute cognitive decline via transient synaptic dysfunction. Radiation Research, 185(4), 423–430. https://doi.org/10.1667/RR14236.1.

Reuter, M., Schmansky, N. J., Rosas, H. D., & Fischl, B. (2012). Within-subject template estimation for unbiased longitudinal image analysis. *NeuroImage, 61*(4), 1402–1418. https://doi.org/10.1016/j.neuroimage.2012.02.084.

Santos-Filho, C., de Lima C. M., Foro C. A., de Oliveira M. A., Magalhaes N. G., Guerreiro-Diniz C., et al. (2014). Visuospatial learning and memory in the Cebus apella and microglial morphology in the molecular layer of the dentate gyrus and CA1 lacunosum molecular layer. Journal of Chemical Neuroanatomy, 61-62(176–188. https://doi.org/10.1016/j.jchemneu.2014.10.001.

Seibert, T. M., Karunamuni R., Bartsch H., Kaifi S., Krishnan A. P., Dalia Y., et al. (2017). Radiation dose-dependent hippocampal atrophy detected with longitudinal volumetric magnetic resonance imaging. International Journal of Radiation Oncology, Biology, Physics, 97(2), 263–269. https://doi.org/10.1016/j.ijrobp.2016.10.035.

Simo, M., Vaquero L., Ripolles P., Gurtubay-Antolin A., Jove J., Navarro A., et al. (2016). Longitudinal brain changes associated with prophylactic cranial irradiation in lung Cancer. Journal of Thoracic Oncology, 11(4), 475–486. https://doi.org/10.1016/j.jtho.2015.12.110.

Small, S. A., Schobel, S. A., Buxton, R. B., Witter, M. P., & Barnes, C. A. (2011). A pathophysiological framework of hippocampal dysfunction in ageing and disease. *Nature Reviews Neuroscience, 12*(10), 585–601. https://doi.org/10.1038/nrn3085.

Son, Y., Yang, M., Wang, H., & Moon, C. (2015). Hippocampal dysfunctions caused by cranial irradiation: A review of the experimental evidence. *Brain, Behavior, and Immunity, 45*, 287–296. https://doi.org/10.1016/j.bbi.2015.01.007.

Sun, Y., Yu X. L., Luo W., Lee A. W., Wee J. T., Lee N., et al. (2014). Recommendation for a contouring method and atlas of organs at risk in nasopharyngeal carcinoma patients receiving intensity-modulated radiotherapy. Radiotherapy and Oncology, 110(3), 390–397. https://doi.org/10.1016/j.radonc.2013.10.035.

Team, R. C. (2014). *R: A language and environment for statistical computing*. Vienna, Austria: R Foundation for Statistical Computing.

Torre, L. A., Bray, F., Siegel, R. L., Ferlay, J., Lortet-Tieulent, J., & Jemal, A. (2015). Global cancer statistics, 2012. *CA: a Cancer Journal for Clinicians, 65*(2), 87–108. https://doi.org/10.3322/caac.21262.

Van Leemput, K., Bakkour A., Benner T., Wiggins G., Wald L. L., Augustinack J., et al. (2009). Automated segmentation of hippocampal subfields from ultra-high resolution in vivo MRI. Hippocampus, 19(6), 549–557. https://doi.org/10.1002/hipo.20615.

Warrington, J. P., Csiszar A., Johnson D. A., Herman T. S., Ahmad S., Lee Y. W., et al. (2011). Cerebral microvascular rarefaction induced by whole brain radiation is reversible by systemic hypoxia in mice. American Journal of Physiology-Heart and Circulatory Physiology, 300(3), H736-H744. https://doi.org/10.1152/ajpheart.01024.2010.

Yao, J. J., Yu X. L., Zhang F., Zhang W. J., Zhou G. Q., Tang L. L., et al. (2017). Radiotherapy with neoadjuvant chemotherapy versus concurrent chemoradiotherapy for ascending-type nasopharyngeal carcinoma: A retrospective comparison of toxicity and prognosis. Chinese Journal of Cancer, 36(1), 26. https://doi.org/10.1186/s40880-017-0195-6.